

Article

Detrended cross-correlations and their random matrix limit: an example from the cryptocurrency market

Stanisław Drożdż ^{1,2,*} , Paweł Jarosz ² , Jarosław Kwapien ¹ , Maria Skupień ³ , Marcin Wątorek ² 
¹ Complex Systems Theory Department, Institute of Nuclear Physics, Polish Academy of Sciences, ul. Radzikowskiego 152, 31-342 Kraków, Poland;

² Faculty of Computer Science and Mathematics, Cracow University of Technology, ul. Warszawska 24, 31-155 Kraków, Poland;

³ Department of Mathematics, University of the National Education Commission, Podchorążych 2, 30-084, Kraków, Poland;

* Correspondence: marcin.watorek@pk.edu.pl; stanislaw.drozd@ifj.edu.pl;

Abstract

Correlations in complex systems are often obscured by nonstationarity, long-range memory, and heavy-tailed fluctuations, which limit the usefulness of traditional covariance-based analyses. To address these challenges, we construct scale and fluctuation-dependent correlation matrices using the multifractal detrended cross-correlation coefficient ρ_r that selectively emphasizes fluctuations of different amplitudes. We examine the spectral properties of these detrended correlation matrices and compare them to the spectral properties of the matrices calculated in the same way from synthetic Gaussian and q Gaussian signals. Our results show that detrending, heavy tails, and the fluctuation-order parameter r jointly produce spectra, which substantially depart from the random case even under absence of cross-correlations in time series. Applying this framework to one-minute returns of 140 major cryptocurrencies from 2021–2024 reveals robust collective modes, including a dominant market factor and several sectoral components whose strength depends on the analyzed scale and fluctuation order. After filtering out the market mode, the empirical eigenvalue bulk aligns closely with the limit of random detrended cross-correlations, enabling clear identification of structurally significant outliers. Overall, the study provides a refined spectral baseline for detrended cross-correlations and offers a promising tool for distinguishing genuine interdependencies from noise in complex, nonstationary, heavy-tailed systems.

Keywords: Multifractal cross-correlations; Detrended cross-correlation analysis; random matrix theory; eigenvalue spectra; cryptocurrency market

1. Introduction

Correlations among complex systems' components play a central role in understanding their collective dynamics [1]. In fields ranging from finance [2–4], climatology [5–8], molecular and biological systems [9,10] to neuroscience [11–13], and physics [14], correlation matrices serve as key tools for quantifying interdependencies between multivariate time series. However, the presence of nonstationarities and long-range dependencies in empirical data often leads to spurious correlations, challenging traditional covariance-based analyses [15–17]. To address these issues, detrended cross-correlation analysis (DCCA) [18] and its generalizations [19–21] have been developed as robust methods for quantifying power-law cross-correlations between nonstationary signals.



Received:

Revised:

Accepted:

Published:

Citation: . Detrended

cross-correlations and their random matrix limit. *Entropy* **2025**, *1*, 0.

<https://doi.org/>
Copyright: © 2025 by the authors.

Licensee MDPI, Basel, Switzerland.

This article is an open access article distributed under the terms and conditions of the Creative Commons Attribution (CC BY) license

(<https://creativecommons.org/licenses/by/4.0/>).

Correlation analysis-based methods are widely used in financial markets. They have been successfully applied to stock markets [22–29], forex [30–34], cryptocurrencies [35–44], and even NFT tokens [45]. These methods are useful in trading, risk management and portfolio optimization [40,41,46–51].

In this work, we study the spectral properties of matrices constructed from detrended cross-correlation coefficients ρ_r (also denoted in literature as ρ_q), which generalize the detrended cross-correlation coefficient ρ_{DCCA} [21], which is an equivalent of the Pearson cross-correlation for the detrended fluctuation analysis [52]. Each element of the resulting matrix captures the scale-dependent correlation between detrended fluctuations of two time series, controlled by the parameter r that governs sensitivity to fluctuation amplitudes. This approach allows us to explore interdependencies in systems characterized by heterogeneous scaling behaviors or multifractality, going beyond the scope of linear correlation measures.

Our primary interest lies in the eigenvalue spectra of such detrended correlation matrices. In conventional correlation matrix theory, the Marčenko–Pastur (M-P) distribution provides the null hypothesis for the eigenvalue density when entries are independent and identically distributed random variables, i.e. when no genuine correlations are present [53]. However, when matrix elements are derived from detrended cross-correlations, the statistical structure may differ substantially from that assumed by the M-P framework. The detrending procedure introduces scale-dependent filtering and residual cross-structure even under nominally uncorrelated conditions. Consequently, the classical random matrix limit cannot be directly applied as a baseline for identifying significant correlations.

We therefore investigate the eigenvalue spectra of the detrended correlation matrices, constructed from the ensemble of synthetic time series representing Gaussian and q Gaussian models [54]. We aim to characterize how detrending and fluctuation-based weighting modify the spectral density and the onset of collective modes. The results provide insights into the appropriate null hypotheses for spectral analysis of detrended correlations and offer a refined framework for distinguishing genuine collective behavior from stochastic background fluctuations in complex systems.

As a practical application of this formalism, we analyze a representative set of the most liquid 140 cryptocurrencies from Binance exchange [55]. The cryptocurrency market provides a particularly suitable testing ground for detrended correlation analysis due to its pronounced nonstationarity, strong cross-dependencies, and heterogeneity in trading activity and capitalization [56]. Price series of digital assets exhibit complex temporal structures, including volatility clustering [57–64] and multifractal scaling [65–72], which render standard correlation measures inadequate. Their price changes are also susceptible to external influences from other financial markets [58,73–80], as well as geopolitical shocks [81–84] or social media impact [85,86].

By constructing the detrended correlation matrix $\rho_r(s)$ from the $\rho_r(s)$ coefficients computed across multiple time scales s , we are able to probe the underlying architecture of interdependencies among these assets while suppressing the influence of global trends and nonstationary effects. Examination of the eigenvalue spectra reveals the presence of collective modes associated with market-wide behavior, sectoral groupings, and noise-dominated components. Comparing these empirical spectra with the corresponding limits derived for uncorrelated signals allows us to identify statistically significant deviations indicative of genuine market structure. This approach thus offers a refined spectral perspective on the collective dynamics and information flow within the cryptocurrency market.

2. Methods

2.1. Detrended cross-correlations

We start from a set of time series: $U_i = \{u_i(j)\}_{j=1}^T$ with $i = 1, \dots, N$. For each time series, a corresponding signal profile is constructed by integrating the data along the time axis:

$$\bar{u}_i(k) = \sum_{j=1}^k u_i(j), \quad k = 1, \dots, T. \quad (1)$$

Next, for a given scale s , this signal profile is divided into $2M_s$ non-overlapping windows of width s starting from both ends of the time series, and, subsequently, it is detrended by best-fitting a polynomial $P_v^{(m)}$ of order m in each window v individually:

$$x_i(sv + k) = \bar{u}_i(sv + k) - P_v^{(m)}(k), \quad k = 1, \dots, s, \quad v = 0, \dots, 2M_s - 1. \quad (2)$$

By proceeding along this way with all time series, we obtain a set of the detrended time series X_i , where $i = 1, \dots, N$ that will be subject to further analysis. Signal covariance is then calculated in each window:

$$f_{ij}^2(s, v) = \frac{1}{s} \sum_{k=1}^s x_i(sv + k)x_j(sv + k), \quad i, j = 1, \dots, N, \quad (3)$$

which becomes variance if $i = j$. In order to allow for a multiscale analysis, a parameter $r \in \mathbb{R}$ is introduced and a family of bivariate r -fluctuation functions is introduced:

$$F_{ij}^r(s) = \frac{1}{2M_s} \sum_{v=0}^{2M_s-1} \text{sign}[f_{ij}^2(s, v)] |f_{ij}^2(s, v)|^{r/2}, \quad (4)$$

where sign of each covariance is preserved while the modulus allows us to avoid complex values if $f_{ij}^2(s, v) < 0$ and $r/2$ is not integer [87]. These functions become univariate if $i = j$. Based on Eq. (4), it is possible to define an r -dependent detrended cross-correlation coefficient [52]:

$$\rho_r^{ij}(s) = \frac{F_{ij}^r(s)}{\sqrt{F_{ii}^r(s)F_{jj}^r(s)}}, \quad (5)$$

whose values $-1 \leq \rho_r^{ij}(s) \leq 1$ have similar interpretation as the Pearson cross-correlation coefficient in the case of $r > 0$. However, by considering different values of r , we are able to focus on the cross-correlations among specific range of fluctuation amplitudes: large-amplitude fluctuation contribution is amplified if $r > 2$ and small-amplitude fluctuation contribution is amplified if $r < 2$.

For a given set of time series, the coefficient $\rho_r^{ij}(s)$ is symmetric with respect to time series order and it can be calculated for all pairs (i, j) with $j = i + 1, \dots, N$. An r -dependent detrended cross-correlation matrix is then constructed as

$$\boldsymbol{\rho}_r(s) = [\rho_r^{ij}(s)]_{i,j=1}^N. \quad (6)$$

The whole procedure from the detrending step to the matrix construction can be repeated for different scales s in some range $s_{\min} \leq s \leq s_{\max}$.

2.2. Spectral characteristics of the detrended cross-correlation matrix

Spectral properties of $\boldsymbol{\rho}_r$ can be determined by solving the eigenvalue problem:

$$\boldsymbol{\rho}_r(s) \mathbf{v}_i(s) = \lambda_i(s) \mathbf{v}_i(s), \quad i = 1, \dots, N, \quad (7)$$

where the ordering is such that $\lambda_1 \geq \lambda_2 \geq \dots \geq \lambda_N$. While the eigenvalues of ρ_r are real-valued owing to the symmetry of the matrix, this matrix is not necessarily positive semi-definite. First, let us look at the simplest case of $r = 2$ and construct a matrix of the fluctuation functions (4) for all pairs of the time series:

$$\mathbf{F}^2(s) = \frac{1}{M_s} \sum_{\nu} \mathbf{f}^2(s, \nu) = \frac{1}{M_s} \sum_{\nu} \frac{1}{s} \mathbf{X}_{\nu}^T(s) \mathbf{X}_{\nu}(s) = \frac{1}{T} \mathbf{X}^T(s) \mathbf{X}(s), \quad (8)$$

where \mathbf{X}_{ν} is a data matrix created from all time series in a window ν and \mathbf{X} is an analogous data matrix for the whole time series (to simplify notation, we assume that their length T is a multiple of s). A dependence of \mathbf{X} on scale s comes from the fact that detrending a signal with a polynomial of a given degree leaves the more trend in the residual signal the larger the scale s is. Since it can be expressed as the product $\mathbf{X}^T \mathbf{X}$, the matrix \mathbf{F}^2 is positive semi-definite.

Now, let us consider the case of $r = 2n$, $n \in \mathbb{N}$, in which

$$\mathbf{F}^{2n}(s) = \frac{1}{M_s} \sum_{\nu} [\mathbf{f}^2(s, \nu)]^{\circ n} = \frac{1}{M_s} \sum_{\nu} \frac{1}{s^n} [\mathbf{X}_{\nu}^T(s) \mathbf{X}_{\nu}(s)]^{\circ n}, \quad (9)$$

where $[\cdot]^{\circ n}$ denotes the Hadamard product of n matrices \cdot (i.e., their element-wise multiplication). It can be shown that this operation preserves the property of positive semi-definiteness (the Schur theorem [88]). A sum of matrices preserves the positive semidefiniteness of the components, therefore there exists a matrix $\tilde{\mathbf{X}}(s)$ such that

$$\mathbf{F}^{2n}(s) = \frac{1}{s^n M_s} \tilde{\mathbf{X}}^T(s) \tilde{\mathbf{X}}(s). \quad (10)$$

This is generally not true for $r \neq 2n$, however. If this is the case, a condition $r/2 \geq N - 2$ must hold to guarantee positive semi-definiteness of $\mathbf{F}^r(s)$ as stated by the FitzGerald-Horn theorem [89]. Otherwise, this matrix may have negative eigenvalues. When they are negative indeed and when the whole spectrum is non-negative is a delicate question: typically, the smaller is r (especially if $r < 1$), the larger is the probability that some eigenvalues fall below 0. The opposite is true if r increases and, eventually, the matrix enters the $r/2 \geq N - 2$ region. Finally, based on Eq. (5), we arrive at the conclusion that $\rho_r(s)$ is positive semi-definite if $\mathbf{F}^r(s)$ reveals this property.

2.3. Random matrix limit and departures

The property of positive semi-definiteness of $\rho_r(s)$ is important from the statistical point of view, because we may then ask a question how is a given matrix related to the Wishart ensemble of random correlation matrices \mathbf{W} [90]. In the absence of genuine cross-correlations in \mathbf{X} , this relation is straightforward for $r = 2$, because the structure of $\mathbf{F}^2(s)$ is in this situation similar to the structure of a Pearson correlation matrix. However, for $r \neq 2$ the matrix structure of $\rho_r(s)$ requires applying of different random matrix ensembles.

If the Wishart case is valid, there is a well-defined distribution of eigenvalues of a matrix constructed for a set of uncorrelated Gaussian-distributed time series in the thermodynamical limit $N, T \rightarrow \infty$, $T/N = Q = \text{const}$ (the Marčenko-Pastur distribution [53]):

$$\phi_W(\lambda) = \frac{1}{2\pi Q\lambda} \sqrt{(\lambda_{\max} - \lambda)(\lambda - \lambda_{\min})}, \quad \lambda_{\min} \leq \lambda \leq \lambda_{\max}, \quad (11)$$

where $\lambda_{\min} = (1 - \sqrt{Q})^2$ and $\lambda_{\max} = (1 + \sqrt{Q})^2$.

In the case of detrended correlations considered here, however, some deviations from the M-P distribution may arise even for random series due to detrending of fluctuations [16].

The space for such deviations increases with increasing the range of detrending (longer scale s). To obtain appropriate null hypotheses for the empirical correlations under consideration, in the absence of analytical formulas for the eigenvalue distributions of correlation matrices constructed in such a generalized manner, numerical simulations are necessary. Therefore, such simulated eigenvalue distributions will be conducted in parallel to such analyses for the empirical data.

Another factor that, in the presence of detrending, may lead to further modification of the above characteristics is the fluctuation distributions of the analyzed time series. Distributions of fluctuations of time series representing many natural phenomena develop thicker tails than the ones obeying the normal distribution. For instance, the distributions of fluctuations in financial rates of return on short time scales quite universally [91] satisfy the so-called inverse-cubic power law [92] and this applies even to the cryptocurrency markets [35,93,94]. Such distributions are quite efficiently described by functions called q Gaussians [95].

2.4. q Gaussian distribution

In general q Gaussian distributions provide a highly practical analytical framework for modeling the corresponding probability distributions. They constitute a natural extension of the standard Gaussian distribution in analogy of how the Tsallis entropy S_q extends the classical Boltzmann-Gibbs entropy S [54,96]. This class of distributions \mathcal{G}_q is characterized by two parameters: a shape parameter $q \in (-\infty, 3)$ and a scale (width) parameter $\beta > 0$. The corresponding probability density function (PDF) assumes the form [54]:

$$\phi_q(x) = \frac{\sqrt{\beta}}{C_q} e_q(-\beta x^2), \quad (12)$$

where $e_q(x)$ denotes the q -exponential function

$$e_q(x) = \begin{cases} (1 + (1-q)x)^{1/(1-q)} & \text{if } q \neq 1 \text{ and } 1 + (1-q)x > 0 \\ 0 & \text{if } q \neq 1 \text{ and } 1 + (1-q)x \leq 0 \\ e^x & \text{if } q = 1, \end{cases} \quad (13)$$

and $C_q = \int_{-\infty}^{\infty} e_q(x^2) dx$ is a normalization constant.

Asymptotic behavior at large $|x|$ of a q Gaussian for $q = 3/2$ then corresponds to the inverse-cubic power law [97].

2.5. Outlying eigenvalues and collectivity

The above considerations concern a set of independently generated random time series, within and between which there are no synchronous correlations. However, the essence of real, natural complex systems is the coexistence of randomness with collective synchronous effects. For fundamental and practical reasons, the latter are, of course, the primary object of interest. Within the general formalism of correlation matrices, such effects manifest themselves in significant deviations from the spectrum of eigenvalues assumed by the appropriate null hypothesis as indicated above. More specifically [98–100], when coherent or collective behavior arises, it effectively reduces the rank of the correlation matrix: a small number of dominant modes capture most of the system's variance, while the remaining degrees of freedom behave as random noise. This reduced rank is reflected in the presence of a few large eigenvalues that stand well above the random matrix bounds, separating them from the random bulk of the spectrum. Such spectral segregation reveals the emergence of collective dynamics and the formation of correlated groups or patterns within the system. In this way, deviations from full-rank randomness — i.e., the appearance

of a low effective rank — serve as a quantitative signature of collective effects and organized structure emerging from an otherwise random background.

3. Data

The empirical dataset consists of $N = 140$ exchange rates for the most actively traded cryptocurrencies, quoted in USDT on the Binance exchange [55]. It covers the period from January 1, 2021, to September 30, 2024, with data publicly available in an open repository [101]. The time series were recorded at a 1 min sampling frequency and transformed into logarithmic returns $R(t_k) = \ln p(t_{k+1}) - \ln p(t_k)$, where $k = 1, \dots, T$.

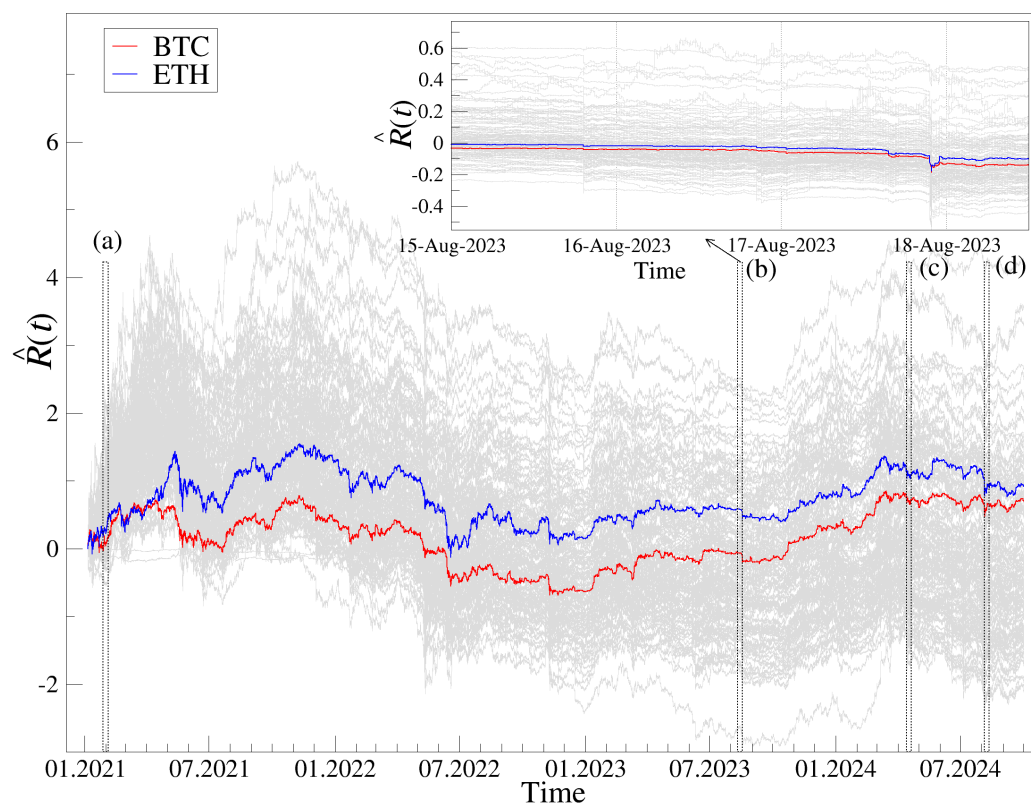


Figure 1. (Main) Evolution of the cumulative log-returns $\hat{R}_i(t_k)$ of the 140 cryptocurrencies over the whole time period from Jan 1, 2021 to Sep 30, 2024. The bulk of the cryptocurrencies is shown in the background (grey lines), while BTC and ETH are distinguished by red and blue lines, respectively. Four specific periods are distinguished by narrow vertical rectangles (a)–(d). (Inset) Evolution of the same data during a selected shorter period (b): Aug 15, 2023 to Aug 18, 2023.

In order for the relative price changes to be directly comparable, the evolution of the cumulative logarithmic returns $\hat{R}_i(t_k) = \sum_{k=1}^T R_i(t_k)$ of the $N = 140$ cryptocurrencies considered here indexed by i ($i = 1, \dots, N$) over the analyzed time period is presented in Fig. 1. Various phases of the market can be observed. The bull market in 2021, then the bear market in 2022 with the crash in May 2022. After reaching its bottom at the end of 2022, the market was in a slower growth phase until mid-2024, then moved sideways until the end of September 2024. Thus, the selected dataset allows for market analysis under various conditions.

From the above rates of return their fluctuation distributions can be directly generated. In the complementary cumulative distribution function (CCDF) representation they are displayed in Fig. 2. As can be seen from the also shown comparison to the corresponding theoretical references, a very good fit of this distribution is obtained in terms of the q Gaussian with $q = 3/2$ which not only provides an overall good fit but also asymptotically corresponds to the inverse cubic law.

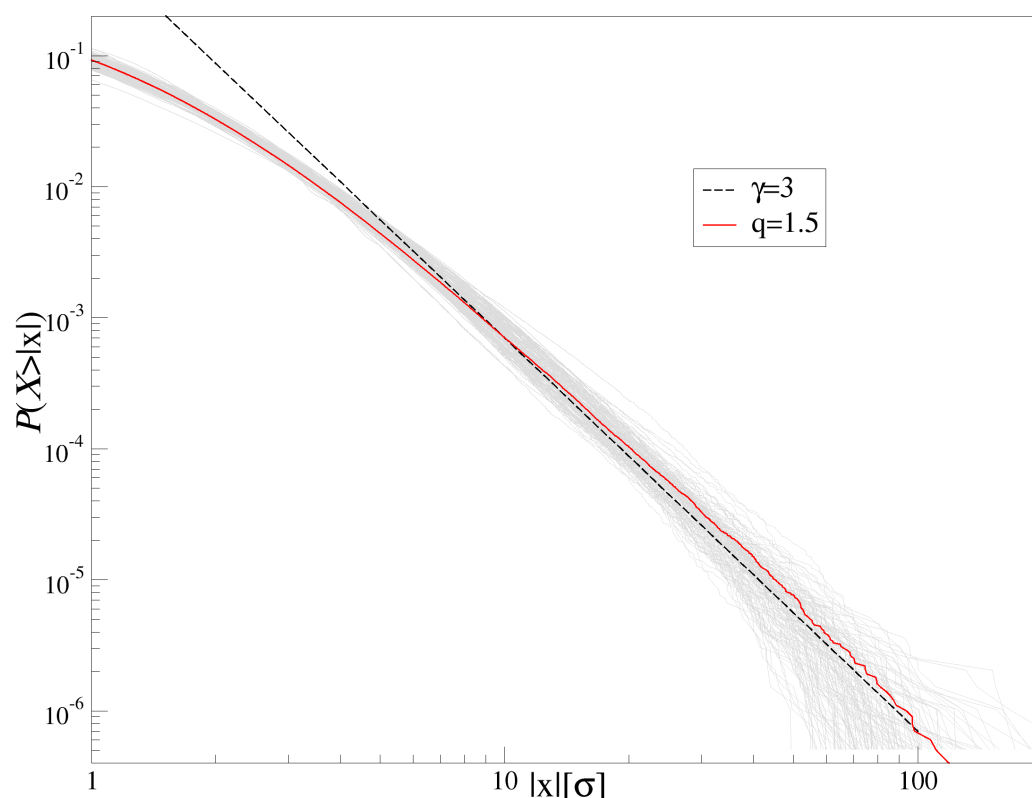


Figure 2. Complementary cumulative distribution function (CCDF) of the log-returns $R_i(t_k)$ for all 140 cryptocurrencies together with q Gaussian ($q = 3/2$) and power law ($\gamma = 3$) CCDFs.

The richness of the dynamics of the set of 140 most actively traded cryptocurrencies considered here is illustrated in Fig. 3, where using a moving 7-day window (with a step of one day), the evolution of the largest eigenvalue λ_1 of the corresponding matrix $\rho_r(s)$ for $r = 2$ and $r = 4$ and three different values of the detrending scale ($s=10, 60$, and 360 min) is shown. As can be seen, λ_1 strongly depends on the window location and, in some places, exhausts a large part of the maximum possible value equal to the trace of the matrix which in this case equals 140. In the vast majority of cases, λ_1 is larger for $r = 2$ case matrix than for $r = 4$, which means that cross-correlations occur here rather at the level of fluctuations with medium amplitude. However, it happens, especially in the later part of the time period considered here, that λ_1 for $r = 4$ takes higher values, which signals the dominance of cross-correlation at the level of larger fluctuation amplitudes. A more detailed inspection indicates that this is associated with more rapid price changes in the cryptocurrency market at such moments. It should also be noted that on average the value of λ_1 increases for increasingly larger detrending scales which is an effect reminiscent of the Epps effect [102–104].

4. Detrended correlation matrices from random series

Even for random series, the form of the cross-correlation matrix depends significantly on the parameter r , on the detrending scale s , and on the fluctuation distributions of these series. As representative examples the synthetic 140 random series of length 10,080 data points (the same as the length of the empirical series) generated from q Gaussian distributions, for three values $q = 1$, which corresponds to the normal distribution, $q = 3/2$, which corresponds to the inverse-cubic power law satisfied by the empirical data considered, and for $q = 2$, which corresponds to fluctuations already in the Lévy-stable regime are used here.

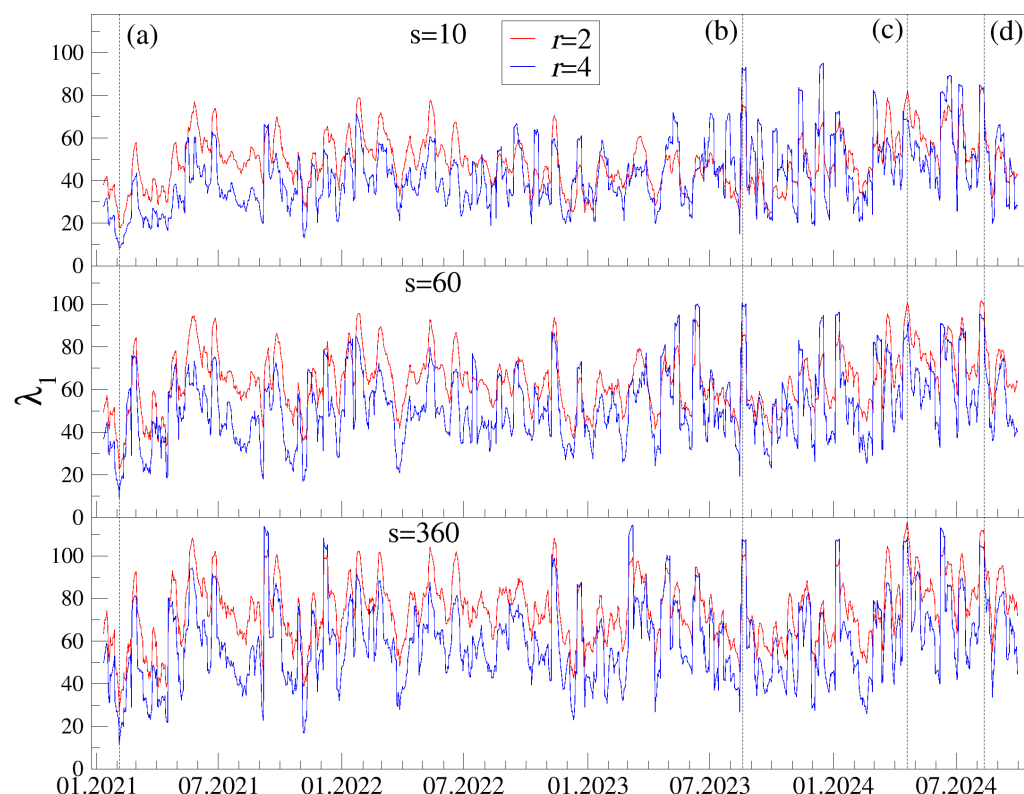


Figure 3. Time evolution of the largest eigenvalue λ_1 of the matrix $\rho_r(s)$ with $r = 2$ (red) and $r = 4$ (blue) for $s = 10$ (top), $s = 60$ (middle), and $s = 360$ (bottom). A rolling window of length 7 days, shifted by 1 day, was applied. Four specific periods are marked by vertical dashed lines (a)–(d).

4.1. Distribution of matrix elements

For these three values of q , two significantly different detrending scales s and five values of parameter r from 2 to 10 with step 2, the distributions of off-diagonal entries (diagonals are units by construction) of the corresponding detrended correlation matrix are systematically illustrated in Fig. 4. As can be seen, all these elements are important and the normal distribution of these entries — as for traditional random matrices — is obtained only for $q = 1$, $r = 2$ at small detrending scales s . Otherwise, the probability distributions of these entries develop increasingly fatter tails as q , r , and s increase, although this increase is progressing in a slightly different form for each of these parameters.

Another perspective on these relationships, somewhat complementary, is presented in Fig. 5, where more variants of the scale parameter s are considered. A systematic increase in the thickness of the tails of these off-diagonal entries is visible. In general, such effects signal a reduction in the effective rank of the matrix [99], i.e., the appearance of several large eigenvalues relative to the global bulk, where the dominant portion of small eigenvalues is located.

4.2. Distribution of eigenvalues

What is typically analyzed first in the context of cross-correlation is the eigenvalue spectrum $\{\lambda_i\}_{i=1}^N$ of the corresponding correlation matrix. For the cases of the matrices in Fig. 4 and Fig. 5, the density distributions $\phi(\lambda)$ of the eigenvalues are displayed in Fig. 6 and Fig. 7, respectively. It can be clearly seen that, as the deviations of the off-diagonal element distributions from the normal distribution increase, the departures of the eigenvalue distributions from the M-P distribution increase. The detrending scale s turns out to be more effective in this respect, and for larger values of s , even the maximum $\phi(\lambda)$

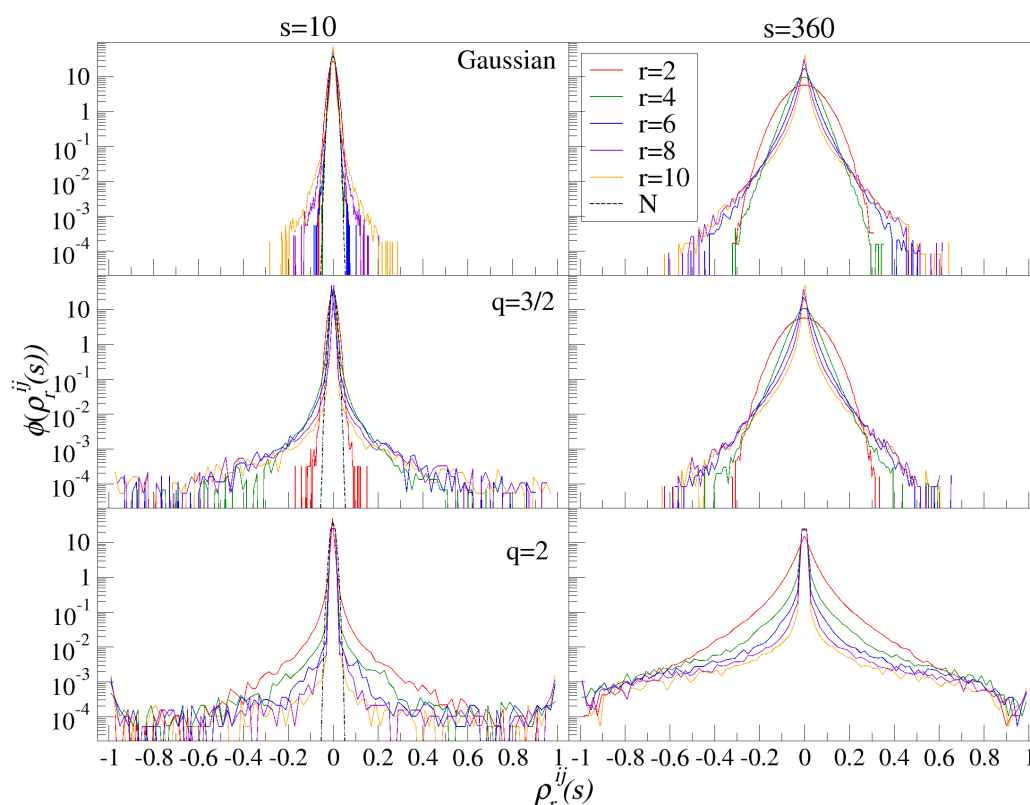


Figure 4. Probability density function (PDF) of the off-diagonal elements of the matrix $\rho_r(s)$ obtained from random uncorrelated time series with q Gaussian distribution defined by $q = 1$ (i.e., a Gaussian distribution, top), $q = 3/2$ (middle), and $q = 2$ (bottom). Results for a few even values of the index r in a range $2 \leq r \leq 10$ and two scales $s = 10$ (left) and $s = 360$ (right) are shown. Each PDF was created from 100 independent realizations of the random data set. The dashed line represents a Gaussian PDF corresponding to random Wishart matrices.

shifts slightly to the left in relation to the M-P distribution. In turn, with a fixed scale, $\phi(\lambda)$ narrows quite significantly towards the M-P distribution with increasing values of the r parameter. Let us recall that all these effects occur already at the level of the set (here 140) of random time series.

5. Cross-correlations in empirical data

Potential real correlations in the empirical data are reflected in the deviations of the characteristics of the respective correlation matrices from the results presented above for the matrices corresponding to random time series. In order to inspect various aspects of such correspondence in varying situations we selected four specific positions of the moving window spanning 7 days, generated the corresponding detrended correlation matrices $\rho_r(s)$ and calculated a complete set of the eigenvalues in each case. The following situations were distinguished: (a) a minimum value of $\lambda_1(r, s, t)$ over the whole period analyzed, which occurred in a window that ends on Feb 4, 2021 (see Fig 3); the position of this minimum was stable across all scales s and for both considered values of the exponent r ; (b) the large-amplitude cross-correlations are significantly stronger than the average ones: $\lambda_1(r = 4) > \lambda_1(r = 2)$ for all considered scales s ; a sample window with such a property ends on Aug 18, 2023; (c) the opposite case of $\lambda_1(r = 2) > \lambda_1(r = 4)$; a sample window with such a property ends on Apr 20, 2024; (d) a sample case of an approximate equality $\lambda_1(r = 2) \approx \lambda_1(r = 4)$, which occurred in a window that ends on Aug 12, 2024. As in the case of the numerical simulations, we consider two even values of the exponent: $r = 2$ and $r = 4$, as well as three scales: $s = 10$ min, $s = 60$ min, and $s = 360$ min.

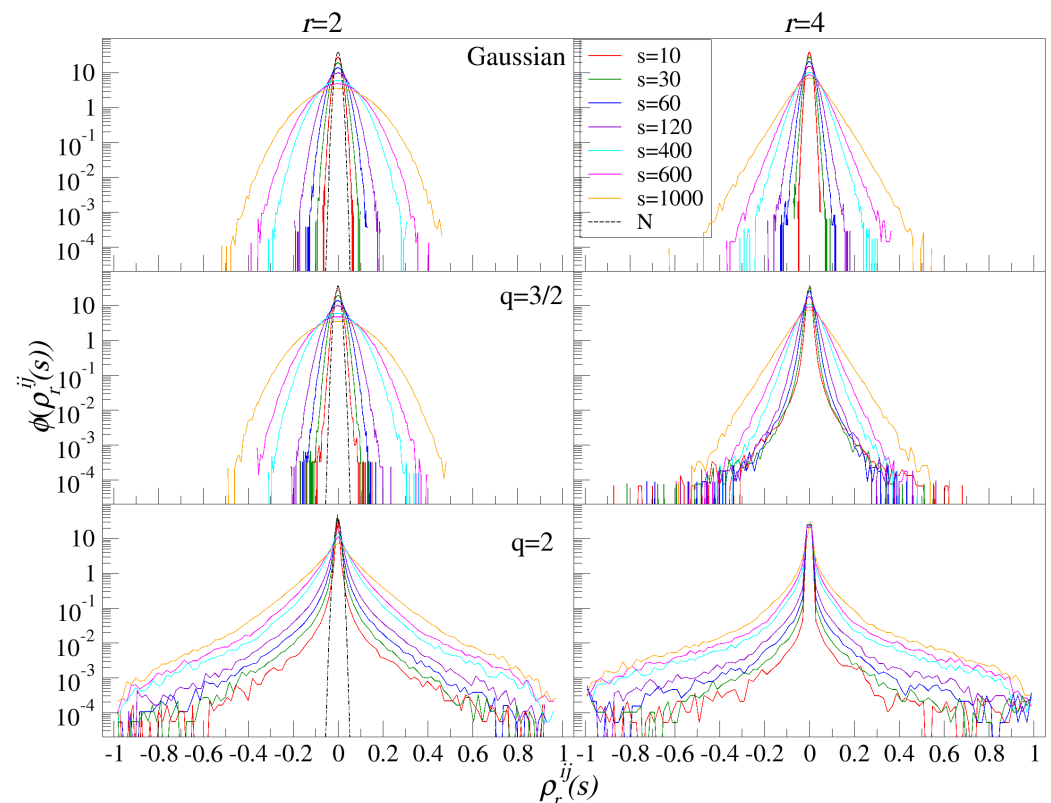


Figure 5. Probability density function (PDF) of the off-diagonal elements of the matrix $\rho_r(s)$ obtained from random uncorrelated time series with q Gaussian distribution defined by $q = 1$ (i.e., a Gaussian distribution, top), $q = 3/2$ (middle), and $q = 2$ (bottom). Results for different scales $10 \leq s \leq 1000$ and for two even values of the index $r = 2$ (left) and $r = 4$ (right) are shown. Each PDF was created from 100 independent realizations of the random data set. The dashed line represents a Gaussian PDF corresponding to random Wishart matrices.

5.1. Distribution of matrix elements

The distributions of the off-diagonal matrix elements of the resulting correlation matrices are displayed in Fig. 8 where their random counterparts for $q = 3/2$ (inverse-cubic power law) are indicated by the red dashed lines. The deviations of the empirical results from the corresponding random ones are very pronounced (and the weakest for case (a)) and consist mainly in the appearance of a large number of sizable matrix elements, many of them even close to unity. These effects signal an effective reduction in the dimension of the leading component of the correlation matrix, i.e., the appearance of one large or at most several larger eigenvalues repelled from many small ones, which are remnants of the random part of this matrix [99].

5.2. Distribution of eigenvalues

The resulting eigenvalue probability density functions for these four cases denoted by (a)-(d) are shown in Fig. 9. These eigenvalue spectra are compared with the corresponding eigenvalue distribution obtained for uncorrelated time series with an inverse cubic power-law pdf ($q = 3/2$, see Fig. 7). The same pattern is always observed: the largest eigenvalue λ_1 is separated from the rest, and the longer the scale s under analysis is, the larger the gap between λ_1 and λ_2 becomes. This result is characteristic of all financial markets, where λ_1 can be associated with the collective movement of prices of all assets (the market factor) and the strength of this collectivity increases as longer return intervals $\Delta t = t_{k+1} - t_k$ are considered. This comes as a natural consequence of delays in the information transfer between the assets stemming from the fact that transactions on different assets

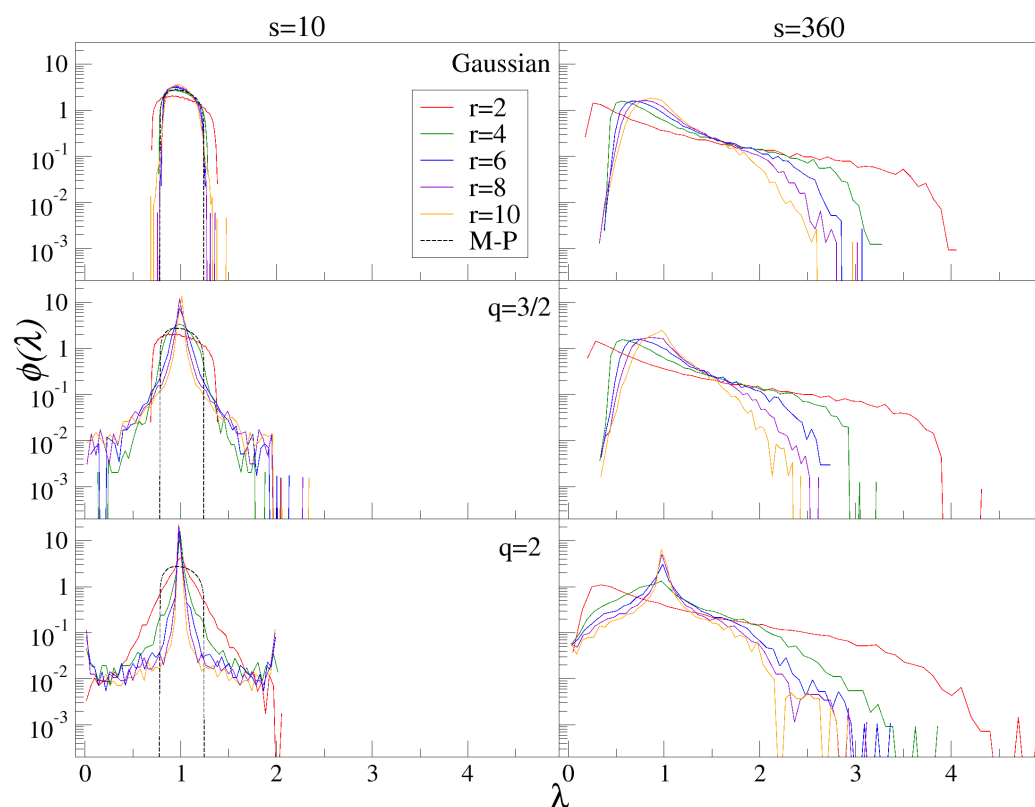


Figure 6. Eigenvalue distribution $\phi(\lambda)$ for the matrix $\rho_r(s)$ obtained from random uncorrelated time series with q Gaussian distribution defined by $q = 1$ (i.e., a Gaussian distribution, top), $q = 3/2$ (middle), and $q = 2$ (bottom). Results for a few even values of the index r in a range $2 \leq r \leq 10$ two scales $s = 10$ (left) and $s = 360$ (right) are shown. Each PDF was created from 100 independent realizations of the random data set. Dashed black line - corresponding Marčenko-Pastur distribution.

are asynchronous and take place at random moments. The market factor is not a unique collective aspect of the cross-correlations among cryptocurrencies: depending on the position of the rolling window on the time axis and on the values of the parameters r and s , a 2nd one or more eigenvalues appear to be larger than it would be expected from the eigenvalue distribution for random data. Such individual detached eigenvalues typically describe the sectoral structure of the market, in which groups of assets are more strongly correlated within the group than outside it. Depending on the specific case, in Fig. 9 the number of such eigenvalues ranges from 1 to 5, with the typical pattern being that for $r = 4$ there are more of them than for $r = 2$. It is worth noting, however, that such eigenvalues lying outside the range predicted for random data also appear below the lower bound λ_{\min} of the random spectrum. In that case, such small eigenvalues describe correlations between individual pairs of assets, without any signs of broader collectivity.

5.3. Filtering out the market factor

An important feature of the spectra shown in almost all panels of Fig. 9 is also a sizable displacement towards zero of the bulk of empirical eigenvalues relative to the corresponding eigenvalue distribution for random data. One of the key causes of this displacement is a fact that when the matrix trace is fixed, the presence of a large, repelled eigenvalue $\lambda_1 \gg \lambda_{\max}$ and several other eigenvalues above λ_{\max} reduces the available range for the remaining eigenvalues, which effectively shifts them leftward (reminiscent of the slaving principle of synergetics [105]). To reduce this effect, it is necessary to filter out

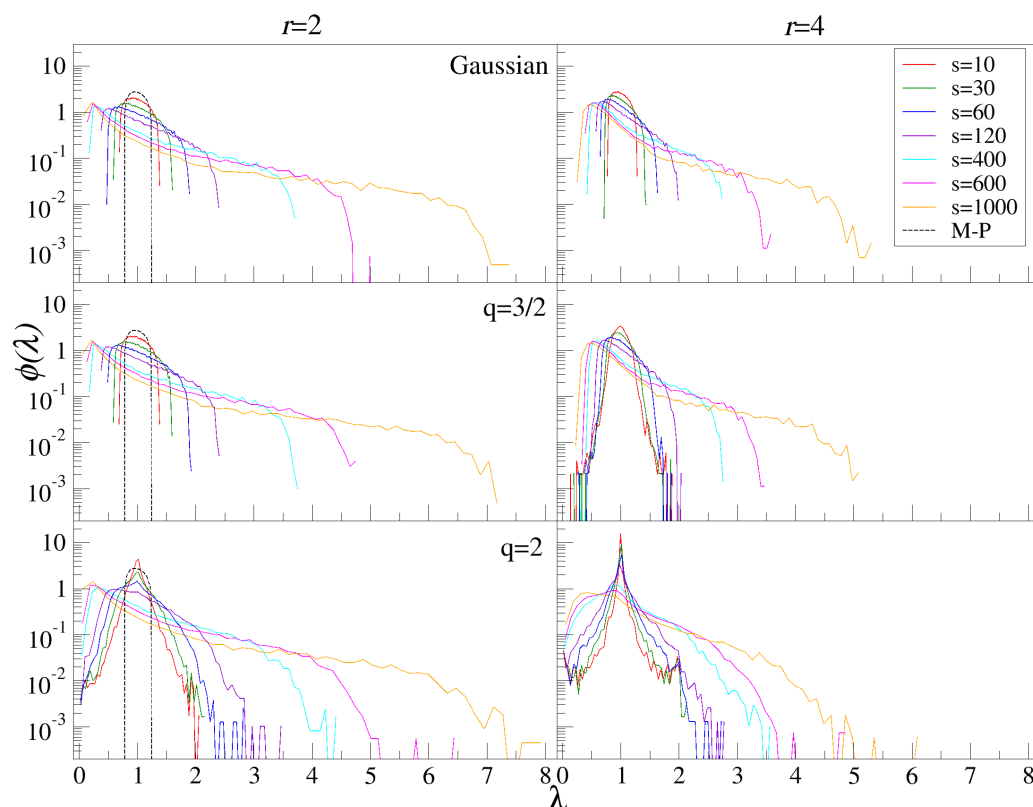


Figure 7. Eigenvalue distribution $\phi(\lambda)$ for the matrix $\rho_r(s)$ obtained from random uncorrelated time series with q Gaussian distribution defined by $q = 1$ (i.e., a Gaussian distribution, top), $q = 3/2$ (middle), and $q = 2$ (bottom). Results for different scales $10 \leq s \leq 1000$ and for two even values of the index $r = 2$ (left) and $r = 4$ (right) are shown. Dashed black line - corresponding Marčenko-Pastur distribution.

the market factor and construct an analogous eigenvalue distribution for the residual data. This can be done by using a regression-based method [1,24]:

$$R_i^{\text{res}}(t_k) = R_i(t_k) - a_i - b_i Z_1(t_k)$$

$$Z_1(t_k) = \sum_{m=1}^N v_{1m} R_m(t_k), \quad (14)$$

where $Z_1(t_k)$ is the contribution to total variance associated with λ_1 and the filtered matrix $\rho'_r(s)$ is constructed from the residual time series $R_i^{\text{res}}(t_k)$ with $i = 1, \dots, N$ and $k = 1, \dots, T$. The results of diagonalization are analogously illustrated in Fig. 10. Indeed, the bulk of the eigenvalues of the empirical correlation matrix coincides quite well with that of the matrix generated from random series with the same detrending scales s and other parameters. Some eigenvalues slightly pushed towards larger values remain and they reflect more local and sectoral cross-correlations.

6. Summary

This study investigates the spectral properties of detrended cross-correlation matrices constructed from the multifractal detrended cross-correlation coefficient $\rho_r(s)$ which generalizes the Pearson correlation to fluctuation-dependent and scale-dependent settings. Because real world multivariate time series — especially financial ones — exhibit strong nonstationarities, heavy-tailed distributions, and long-range dependence, traditional covariance-based correlation matrices often generate misleading structures. To address this, the paper examines how detrending, fluctuation-selection via the parameter r and em-

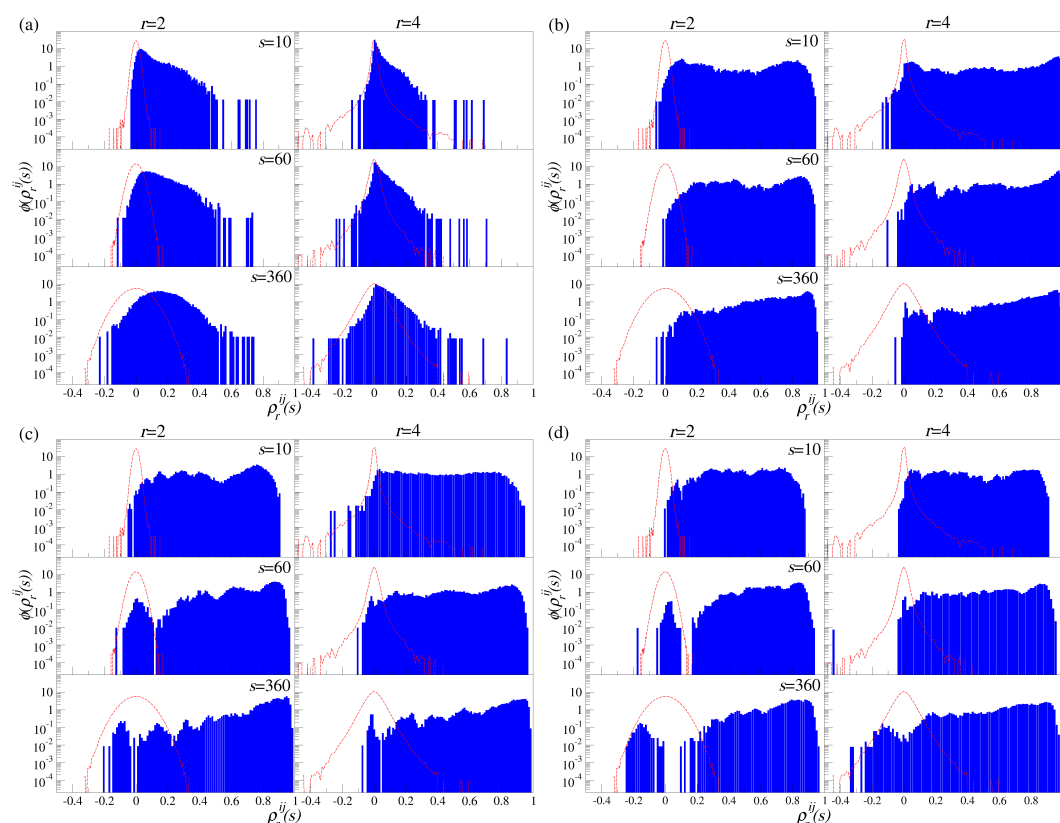


Figure 8. Probability density function of the off-diagonal elements of the empirical matrix $\rho_r(s)$ (histogram) calculated in rolling windows ending on (a) Feb 4, 2021, (b) Aug 18, 2023, (c) Apr 20, 2024, and (d) Aug 12, 2024. In each case, results for three scales: $s = 10$ (top), $s = 60$ (middle), and $s = 360$ (bottom) and for two index values: $r = 2$ (left) and $r = 4$ (right) are shown (histogram) and the corresponding random matrix ensemble (red dashed line). The random case represents a time series with q Gaussian distribution with $q = 3/2$ and s and r parameters corresponding to cases shown in the middle row of Fig. 5.

empirical heavy-tailed distributions collectively influence the eigenvalue spectra of empirical detrended correlation matrices and their counterparts constructed from random time series. Synthetic ensembles of Gaussian and q Gaussian time series are first used to characterize the “null” spectral behavior of detrended correlation matrices. The results show that detrending modifies matrix-element distributions and eigenvalue spectra in systematic ways—most notably by fattening the tails of off-diagonal entries and producing departures from the standard Marčenko–Pastur (M-P) distribution even in fully uncorrelated data. The extent of these deviations grows with the detrending scale s , the fluctuation-order parameter r , and the heaviness of the underlying distribution tails.

The empirical analysis employs 1 min returns of 140 the most liquid cryptocurrencies traded on Binance between 2021 and 2024. Across rolling windows and multiple detrending scales, the leading eigenvalues of the detrended correlation matrices consistently rise above their bounds for uncorrelated time series, indicating strong collective behavior. The dominant mode corresponds to market-wide synchronous motion, while several subleading modes reflect sectoral or structural groupings within the cryptocurrency market. The number and size of these outlying eigenvalues depend on both the temporal scale and the chosen fluctuation order with $r = 4$ generally highlighting cross-correlations among large-amplitude price movements. By filtering out the dominant market mode and reanalyzing the residual covariance structure, the paper demonstrates that the empirical bulk eigenvalue distribution aligns closely with the corresponding null spectra derived

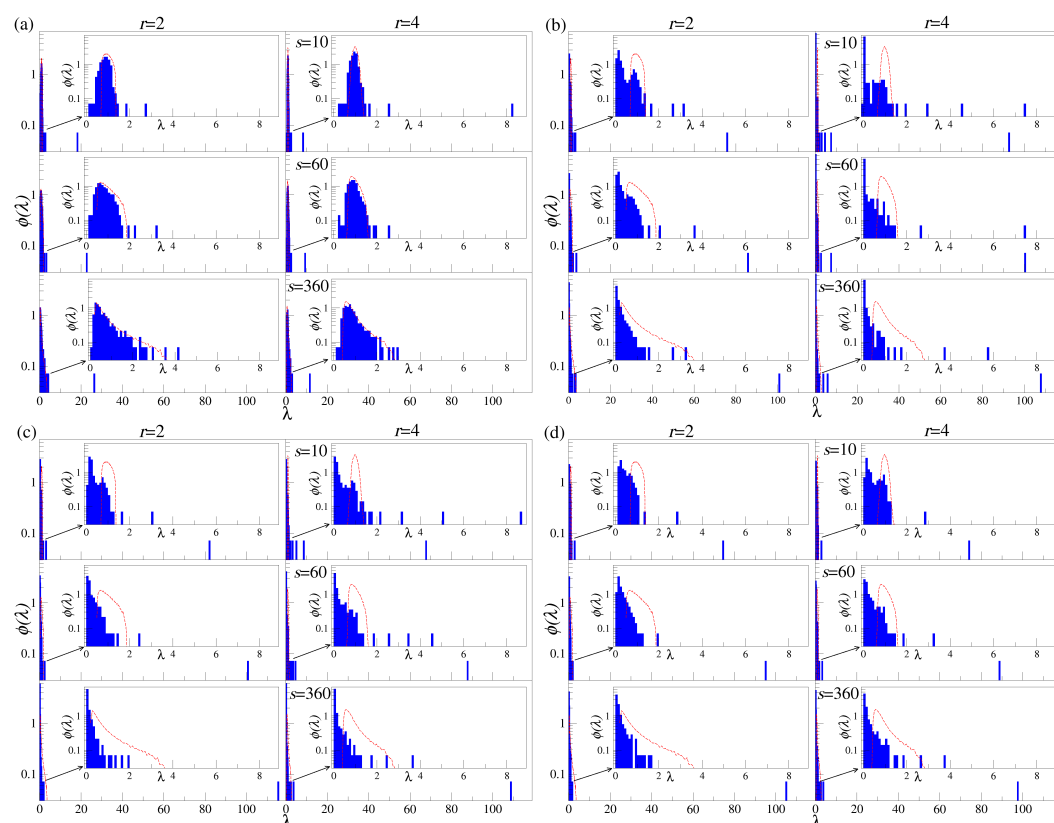


Figure 9. (Main) Eigenvalue distribution $\phi(\lambda)$ for the matrix $p_r(s)$ obtained from the empirical data in rolling windows ending on (a) Feb 4, 2021, (b) Aug 18, 2023, (c) Apr 20, 2024, and (d) Aug 12, 2024. In each case, results for three scales: $s = 10$ (top), $s = 60$ (middle), and $s = 360$ (bottom) and for two index values: $r = 2$ (left) and $r = 4$ (right) are shown (histogram). Eigenvalue distributions representing random data with q Gaussian distribution with $q = 3/2$ and s and r parameters corresponding to cases shown in middle row in Fig. 6 are denoted by red dashed line in each panel. (Inset) Magnification of the bulk- λ region of the main panel.

from detrended random series. The remaining outliers then cleanly reveal local, sector-specific dependencies.

Overall, the work provides a refined spectral benchmark - beyond the classical M-P framework - suitable for systems in which detrending and heavy-tailed fluctuations cannot be neglected. Future research could extend this framework by deriving analytical approximations for the random-matrix limits of detrended correlation spectra, helping to formalize the empirical baselines established in this work.

Author Contributions: Conceptualization, S.D., J.K. and M.W.; methodology, S.D., J.K. and M.W.; software, M.W.; validation, S.D., J.P., J.K. and M.W.; formal analysis, S.D., J.K. and M.W.; investigation, S.D., J.P., J.K., M.S. and M.W.; resources, M.S. and M.W.; data curation, M.S. and M.W.; writing—original draft preparation, S.D. and J.K.; writing—review and editing, S.D., J.P., J.K. and M.W.; visualization, M.S. and M.W.; supervision, S.D.; project administration, S.D., J.P., J.K. and M.W.; funding acquisition, J.P. All authors have read and agreed to the published version of the manuscript.

Funding: This research received no external funding.

Institutional Review Board Statement: Not applicable.

Informed Consent Statement: Not applicable.

Data Availability Statement: The data are available in an open repository [101]

Conflicts of Interest: The authors declare no conflicts of interest.

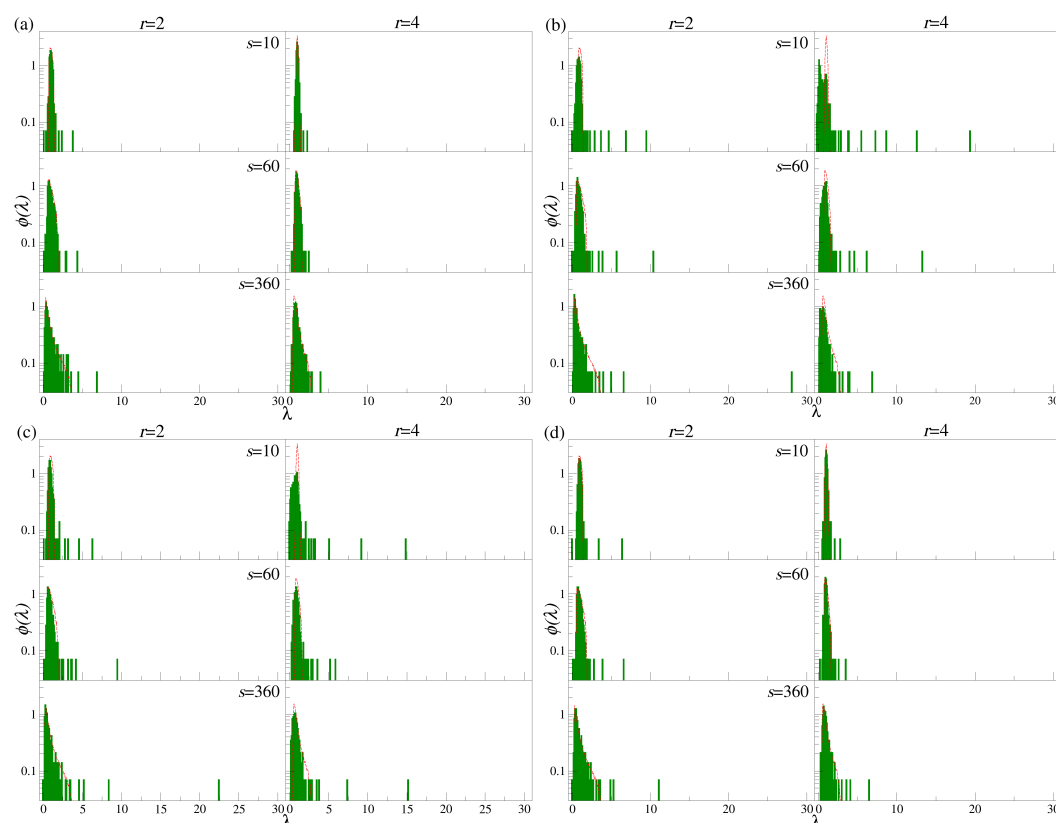


Figure 10. Eigenvalue distribution $\phi(\lambda)$ for the filtered matrix $\rho'_r(s)$ obtained from the empirical data in rolling windows ending on (a) Feb 4, 2021, (b) Aug 18, 2023, (c) Apr 20, 2024, and (d) Aug 12, 2024. In each case, results for three scales: $s = 10$ (top), $s = 60$ (middle), and $s = 360$ (bottom) and for two index values: $r = 2$ (left) and $r = 4$ (right) are shown (histogram). Eigenvalue distributions representing random data with q Gaussian distribution with $q = 3/2$ and s and r parameters corresponding to cases shown in middle row in Fig. 6 are denoted by red dashed line in each panel.

References

1. Kwapień, J.; Drożdż, S. Physical approach to complex systems. *Physics Reports* **2012**, *515*, 115–226. <https://doi.org/10.1016/j.physrep.2012.01.007>.
2. Bun, J.; Bouchaud, J.P.; Potter, M. Cleaning large correlation matrices: tools from random matrix theory. *Physics Reports* **2017**, *666*, 1–109. <https://doi.org/10.1016/j.physrep.2016.10.005>.
3. Jiang, Z.Q.; Xie, W.J.; Zhou, W.X.; Sornette, D. Multifractal analysis of financial markets: A review. *Reports on Progress in Physics* **2019**, *82*, 125901. <https://doi.org/10.1088/1361-6633/ab42fb>.
4. Bardoscia, M.; Barucca, P.; Battiston, S.; Caccioli, F.; Cimini, G.; Garlaschelli, D.; Saracco, F.; Squartini, T.; Caldarelli, G. The physics of financial networks. *Nature Reviews Physics* **2021**, *3*, 490–507. <https://doi.org/10.1038/s42254-021-00322-5>.
5. Srikanthan, R.; McMahon, T.A. Stochastic generation of annual, monthly and daily climate data: A review. *Hydrology and Earth System Sciences* **2001**, *5*, 653–670. <https://doi.org/10.5194/hess-5-653-2001>.
6. Al-Kandari, N.M.; Jolliffe, I.T. Variable selection and interpretation in correlation principal components. *Environmetrics: The official journal of the International Environmetrics Society* **2005**, *16*, 659–672. <https://doi.org/10.1002/env.728>.
7. Feijóo, A.; Villanueva, D. Assessing wind speed simulation methods. *Renewable and Sustainable Energy Reviews* **2016**, *56*, 473–483. <https://doi.org/10.1016/j.rser.2015.11.094>.

8. Mengis, N.; Keller, D.P.; Oschlies, A. Systematic Correlation Matrix Evaluation (SCoMaE) - a bottom-up, science-led approach to identifying indicators. *Earth System Dynamics* **2018**, *9*, 15–31. <https://doi.org/10.5194/esd-9-15-2018>.
9. Dykeman, E.C.; Sankey, O.F. Normal mode analysis and applications in biological physics. *Journal of Physics: Condensed Matter* **2010**, *22*, 423202. <https://doi.org/10.1088/0953-8984/22/42/423202>.
10. Kamberaj, H. A theoretical model for the collective motion of proteins by means of principal component analysis. *Central European Journal of Physics* **2011**, *9*, 96–109. <https://doi.org/10.2478/s11534-010-0048-2>.
11. Kwapień, J.; Drożdż, S.; Joannides, A. Temporal correlations versus noise in the correlation matrix formalism: An example of the brain auditory response. *Physical Review E* **2000**, *62*, 5557–5564. <https://doi.org/10.1103/PhysRevE.62.5557>.
12. de Cheveigné, A.; Di Liberto, G.M.; Arzounian, D.; Wong, D.D.; Hjortkjær, J.; Fuglsang, S.; Parra, L.C. Multiway canonical correlation analysis of brain data. *NeuroImage* **2019**, *186*, 728–740. <https://doi.org/10.1016/j.neuroimage.2018.11.026>.
13. Snyder, A.Z.; Nishino, T.; Shimony, J.S.; Lenze, E.J.; Wetherell, J.L.; Voegtle, M.; Miller, J.P.; Yingling, M.D.; Marcus, D.; Gurney, J.; et al. Covariance and Correlation Analysis of Resting State Functional Magnetic Resonance Imaging Data Acquired in a Clinical Trial of Mindfulness-Based Stress Reduction and Exercise in Older Individuals. *Frontiers in Neuroscience* **2022**, *16*, 825547. <https://doi.org/10.3389/fnins.2022.825547>.
14. Izenman, A.J. Random Matrix Theory and Its Applications. *Statistical Science* **2021**, *36*, 421–442. <https://doi.org/10.1214/20-STS799>.
15. Peng, C.K.; Buldyrev, S.V.; Havtin, S.; Simons, M.; Stanley, H.E.; Goldberger, A.L. Mosaic organization of DNA nucleotides. *Physical Review E* **1994**, *49*, 1685–1689. <https://doi.org/10.1103/PhysRevE.49.1685>.
16. Chen, Z.; Ivanov, P.; Hu, K.; H.E, S. Effect of nonstationarities on detrended fluctuation analysis. *Physical Review E* **2002**, p. 041107. <https://doi.org/10.1103/PhysRevE.65.041107>.
17. Bryce, R.M.; Sprague, K.B. Revisiting detrended fluctuation analysis. *Scientific Reports* **2012**, *2*, 315. <https://doi.org/10.1038/srep00315>.
18. Podobnik, B.; Stanley, H.E. Detrended cross-correlation analysis: A new method for analyzing two nonstationary time series. *Physical Review Letters* **2008**, *100*, 084102. <https://doi.org/10.1103/PhysRevLett.100.084102>.
19. Zhou, W.X. Multifractal detrended cross-correlation analysis for two nonstationary signals. *Physical Review E* **2008**, *77*, 066211. <https://doi.org/10.1103/PhysRevE.77.066211>.
20. Oświęcimka, P.; Drożdż, S.; Forczek, M.; Jadach, S.; Kwapień, J. Detrended cross-correlation analysis consistently extended to multifractality. *Physical Review E* **2014**, *89*, 023305. <https://doi.org/10.1103/PhysRevE.89.023305>.
21. Zebende, G. DCCA cross-correlation coefficient: Quantifying level of cross-correlation. *Physica A* **2011**, *390*, 614–618. <https://doi.org/10.1016/j.physa.2010.10.022>.
22. Drożdż, S.; Gümmer, F.; Górski, A.Z.; Ruf, F.; Speth, J. Dynamics of competition between collectivity and noise in the stock market. *Physica A* **2000**, *287*, 440–449. [https://doi.org/10.1016/S0378-4371\(00\)00383-6](https://doi.org/10.1016/S0378-4371(00)00383-6).
23. Plerou, V.; Gopikrishnan, P.; Rosenow, B.; Amaral, L.; Stanley, H. A random matrix theory approach to financial cross-correlations. *Physica A* **2000**, *287*, 374–382. [https://doi.org/10.1016/S0378-4371\(00\)00376-9](https://doi.org/10.1016/S0378-4371(00)00376-9).
24. Plerou, V.; Gopikrishnan, P.; Rosenow, B.; Amaral, L.A.; Guhr, T.; Stanley, H.E. Random matrix approach to cross correlations in financial data. *Physical Review E* **2002**, *65*, 066126. <https://doi.org/10.1103/PhysRevE.65.066126>.
25. Utsugi, A.; Ino, K.; Oshikawa, M. Random matrix theory analysis of cross correlations in financial markets. *Phys. Rev. E* **2004**, *70*, 026110. <https://doi.org/10.1103/PhysRevE.70.026110>.
26. Wang, G.J.; Xie, C.; Chen, S.; Yang, J.J.; Yang, M.Y. Random matrix theory analysis of cross-correlations in the US stock market: Evidence from Pearson's correlation coefficient and detrended cross-correlation coefficient. *Physica A* **2013**, *392*, 3715–3730. <https://doi.org/10.1016/j.physa.2013.04.027>.

27. Zhao, L.; Li, W.; Fenu, A.; Podobnik, B.; Wang, Y.; Stanley, H.E. The q-dependent detrended cross-correlation analysis of stock market. *Journal of Statistical Mechanics: Theory and Experiment* **2018**, *2018*, 023402. <https://doi.org/10.1088/1742-5468/aa9db0>.
28. James, N.; Menzies, M. Efficiency of communities and financial markets during the 2020 pandemic. *Chaos* **2021**, *31*, 083116. <https://doi.org/10.1063/5.005449>.
29. James, N.; Menzies, M.; Gottwald, G.A. On financial market correlation structures and diversification benefits across and within equity sectors. *Physica A* **2022**, *604*, 127682. <https://doi.org/10.1016/j.physa.2022.127682>.
30. Drożdż, S.; Górski, A.; Kwapień, J. World currency exchange rate cross-correlations. *The European Physical Journal B* **2007**, *58*, 499–502. <https://doi.org/10.1140/epjb/e2007-00246-8>.
31. Mai, Y.; Chen, H.; Zou, J.Z.; Li, S.P. Currency co-movement and network correlation structure of foreign exchange market. *Physica A* **2018**, *492*, 65–74. <https://doi.org/https://doi.org/10.1016/j.physa.2017.09.068>.
32. Gębarowski, R.; Oświęcimka, P.; Wątopek, M.; Drożdż, S. Detecting correlations and triangular arbitrage opportunities in the Forex by means of multifractal detrended cross-correlations analysis. *Nonlinear Dynamics* **2019**, *98*, 2349–2364. <https://doi.org/10.1007/s11071-019-05335-5>.
33. Miśkiewicz, J. Network Analysis of Cross-Correlations on Forex Market during Crises. Globalisation on Forex Market. *Entropy* **2021**, *23*. <https://doi.org/10.3390/e23030352>.
34. Miśkiewicz, J.; Bonarska-Kujawa, D. Evolving Network Analysis of S&P500 Components: COVID-19 Influence of Cross-Correlation Network Structure. *Entropy* **2022**, *24*. <https://doi.org/10.3390/e24010021>.
35. Stosic, D.; Stosic, D.; Luderer, T.B.; Stosic, T. Collective behavior of cryptocurrency price changes. *Physica A* **2018**, *507*, 499–509. <https://doi.org/10.1016/j.physa.2018.05.050>.
36. Basnarkov, L.; Stojkoski, V.; Utkovski, Z.; Kocarev, L. Correlation patterns in foreign exchange markets. *Physica A* **2019**, *525*, 1026–1037. <https://doi.org/https://doi.org/10.1016/j.physa.2019.04.044>.
37. Zięba, D.; Kokoszczynski, R.; Śledzińska, K. Shock transmission in the cryptocurrency market. Is Bitcoin the most influential? *International Review of Financial Analysis* **2019**, *64*, 102–125. <https://doi.org/10.1016/j.irfa.2019.04.009>.
38. Drożdż, S.; Minati, L.; Oświęcimka, P.; Stanuszek, M.; Wątopek, M. Competition of noise and collectivity in global cryptocurrency trading: Route to a self-contained market. *Chaos* **2020**, *30*, 023122. <https://doi.org/10.1063/1.5139634>.
39. Briola, A.; Aste, T. Dependency Structures in Cryptocurrency Market from High to Low Frequency. *Entropy* **2022**, *24*, 1548. <https://doi.org/10.3390/e24111548>.
40. James, N.; Menzies, M. Collective correlations, dynamics, and behavioural inconsistencies of the cryptocurrency market over time. *Nonlinear Dynamics* **2022**, *107*, 4001–4017. <https://doi.org/10.1007/s11071-021-07166-9>.
41. James, N. Evolutionary correlation, regime switching, spectral dynamics and optimal trading strategies for cryptocurrencies and equities. *Physica D* **2022**, *434*, 133262. <https://doi.org/10.1016/j.physd.2022.133262>.
42. Jing, R.; Rocha, L.E. A network-based strategy of price correlations for optimal cryptocurrency portfolios. *Finance Research Letters* **2023**, *58*, 104503. <https://doi.org/10.1016/j.frl.2023.104503>.
43. Wątopek, M.; Skupień, M.; Kwapień, J.; Drożdż, S. Decomposing cryptocurrency high-frequency price dynamics into recurring and noisy components. *Chaos* **2023**, *33*, 083146. <https://doi.org/10.1063/5.0165635>.
44. Jin, L.; Zheng, B.; Jiang, X.; Xiong, L.; Zhang, J.; Ma, J. Dynamic cross-correlation in emerging cryptocurrency market. *Physica A* **2025**, *668*, 130568. <https://doi.org/https://doi.org/10.1016/j.physa.2025.130568>.
45. Wątopek, M.; Szydło, P.; Kwapień, J.; Drożdż, S. Correlations versus noise in the NFT market. *Chaos* **2024**, *34*, 073112. <https://doi.org/10.1063/5.0214399>.
46. Cohen, G.; Qadan, M. The complexity of cryptocurrencies algorithmic trading. *Mathematics* **2022**, *10*, 2037. <https://doi.org/10.3390/math10122037>.

47. James, N.; Menzies, M.; Chin, K. Economic state classification and portfolio optimisation with application to stagflationary environments. *Chaos, Solitons & Fractals* **2022**, *164*, 112664. <https://doi.org/10.1016/j.chaos.2022.112664>.
48. James, N.; Menzies, M.; Chan, J. Semi-Metric Portfolio Optimization: A New Algorithm Reducing Simultaneous Asset Shocks. *Econometrics* **2023**, *11*. <https://doi.org/10.3390/econometrics11010008>.
49. Bhattacharjee, P.; Mishra, S.; Kang, S.H. Extreme frequency connectedness, determinants and portfolio analysis of major cryptocurrencies: Insights from quantile time-frequency approach. *The Quarterly Review of Economics and Finance* **2025**, *100*, 101974. <https://doi.org/https://doi.org/10.1016/j.qref.2025.101974>.
50. Sila, J.; Mark, M.; Kristoufek, L.; Weber, T.A. Crypto market betas: the limits of predictability and hedging. *Financial Innovation* **2025**, *11*, 107. <https://doi.org/10.1186/s40854-025-00777-w>.
51. Tsioutsios, A.; Yarovaya, L.; Dimitriou, D. Exploring portfolio diversification with alternative investments: An international TVP-VAR approach. *Research in International Business and Finance* **2025**, *80*, 103143. <https://doi.org/https://doi.org/10.1016/j.ribaf.2025.103143>.
52. Kwapień, J.; Oświęcimka, P.; Drożdż, S. Detrended fluctuation analysis made flexible to detect range of cross-correlated fluctuations. *Physical Review E* **2015**, *92*, 052815. <https://doi.org/10.1103/PhysRevE.92.052815>.
53. Marčenko, V.A.; Pastur, L.A. Distribution of eigenvalues for some sets of random matrices. *Mathematics of the USSR-Sbornik* **1967**, *1*, 457–483. <https://doi.org/10.1070/SM1967v001n04ABEH001994>.
54. Umarov, S.; Tsallis, C.; Steinberg, S. On a q-Central Limit Theorem Consistent with Nonextensive Statistical Mechanics. *Milan Journal of Mathematics* **2008**, *76*, 307–328. <https://doi.org/10.1007/s00032-008-0087-y>.
55. Binance. <https://www.binance.com/>.
56. Wątopek, M.; Drożdż, S.; Kwapień, J.; Minati, L.; Oświęcimka, P.; Stanuszek, M. Multiscale characteristics of the emerging global cryptocurrency market. *Physics Reports* **2021**, *901*, 1–82. <https://doi.org/10.1016/j.physrep.2020.10.005>.
57. Drożdż, S.; Gębarowski, R.; Minati, L.; Oświęcimka, P.; Wątopek, M. Bitcoin market route to maturity? Evidence from return fluctuations, temporal correlations and multiscaling effects. *Chaos* **2018**, *28*, 071101. <https://doi.org/10.1063/1.5036517>.
58. James, N. Dynamics, behaviours, and anomaly persistence in cryptocurrencies and equities surrounding COVID-19. *Physica A* **2021**, *570*, 125831. <https://doi.org/10.1016/j.physa.2021.125831>.
59. Evrim Mandaci, P.; Cagli, E.C. Herding intensity and volatility in cryptocurrency markets during the COVID-19. *Finance Research Letters* **2022**, *46*, 102382. <https://doi.org/10.1016/j.frl.2021.102382>.
60. Nguyen, A.P.N.; Mai, T.T.; Bezbradica, M.; Crane, M. Volatility and returns connectedness in cryptocurrency markets: Insights from graph-based methods. *Physica A* **2023**, *632*, 129349. <https://doi.org/10.1016/j.physa.2023.129349>.
61. Brouty, X.; Garcin, M. Fractal properties, information theory, and market efficiency. *Chaos, Solitons & Fractals* **2024**, *180*, 114543. <https://doi.org/10.1016/j.chaos.2024.114543>.
62. Sila, J.; Kocenda, E.; Kristoufek, L.; Kukacka, J. Good vs. bad volatility in major cryptocurrencies: The dichotomy and drivers of connectedness. *Journal of International Financial Markets, Institutions and Money* **2024**, *96*, 102062. <https://doi.org/https://doi.org/10.1016/j.intfin.2024.102062>.
63. Queiroz, R.; Kristoufek, L.; David, S. A combined framework to explore cryptocurrency volatility and dependence using multivariate GARCH and Copula modeling. *Physica A* **2024**, *652*, 130046. <https://doi.org/https://doi.org/10.1016/j.physa.2024.130046>.
64. Bui, H.Q.; Schinckus, C.; Al-Jaifi, H. Long-range correlations in cryptocurrency markets: A multi-scale DFA approach. *Physica A* **2025**, *661*, 130417. <https://doi.org/10.1016/j.physa.2025.130417>.
65. Takaishi, T. Statistical properties and multifractality of Bitcoin. *Physica A* **2018**, *506*, 507–519. <https://doi.org/10.1016/j.physa.2018.04.046>.

66. Stosic, D.; Stosic, D.; Ludermir, T.B.; Stosic, T. Multifractal behavior of price and volume changes in the cryptocurrency market. *Physica A* **2019**, *520*, 54–61. <https://doi.org/https://doi.org/10.1016/j.physa.2018.12.038>.
67. Takaishi, T.; Adachi, T. Market efficiency, liquidity, and multifractality of Bitcoin: a dynamic study. *Asia-Pacific Financial Markets* **2020**, *27*, 145–154. <https://doi.org/10.1007/s10690-019-09286-0>.
68. Bariviera, A.F. One model is not enough: Heterogeneity in cryptocurrencies' multifractal profiles. *Finance Research Letters* **2021**, *39*, 101649. <https://doi.org/https://doi.org/10.1016/j.frl.2020.101649>.
69. Kwapien, J.; Watorek, M.; Bezbradica, M.; Crane, M.; Tan Mai, T.; Drozd, S. Analysis of inter-transaction time fluctuations in the cryptocurrency market. *Chaos* **2022**, *32*, 083142. <https://doi.org/10.1063/5.0104707>.
70. Kwapien, J.; Watorek, M.; Drozd, S. Multifractal cross-correlations of bitcoin and ether trading characteristics in the post-COVID-19 time. *Future Internet* **2022**, *14*, 215. <https://doi.org/doi.org/10.3390/fi14070215>.
71. Watorek, M.; Królczyk, M.; Kwapien, J.; Stanis, T.; Drozd, S. Approaching Multifractal Complexity in Decentralized Cryptocurrency Trading. *Fractal and Fractional* **2024**, *8*. <https://doi.org/10.3390/fractalfract8110652>.
72. Drozd, S.; Kluszczyński, R.; Kwapien, J.; Watorek, M. Multifractality and Its Sources in the Digital Currency Market. *Future Internet* **2025**, *17*. <https://doi.org/10.3390/fi17100470>.
73. Conlon, T.; McGee, R. Safe haven or risky hazard? Bitcoin during the Covid-19 bear market. *Finance Research Letters* **2020**, *35*, 101607. <https://doi.org/10.1016/j.frl.2020.101607>.
74. Zhang, Y.J.; Bouri, E.; Gupta, R.; Ma, S.J. Risk spillover between Bitcoin and conventional financial markets: An expectile-based approach. *The North American Journal of Economics and Finance* **2021**, *55*, 101296. <https://doi.org/https://doi.org/10.1016/j.najef.2020.101296>.
75. Choi, S.; Shin, J. Bitcoin: An inflation hedge but not a safe haven. *Finance Research Letters* **2022**, *46*, 102379. <https://doi.org/10.1016/j.frl.2021.102379>.
76. Elmelki, A.; Chaabane, N.; Benammar, R. Exploring the relationship between cryptocurrency and S&P500: evidence from wavelet coherence analysis. *International Journal of Blockchains and Cryptocurrencies* **2022**, *3*, 256–268. <https://doi.org/10.1504/IJBC.2022.126287>.
77. Watorek, M.; Kwapien, J.; Drozd, S. Cryptocurrencies are becoming part of the world global financial market. *Entropy* **2023**, *25*, 377. <https://doi.org/10.3390/e25020377>.
78. Kristjanpoller, W.; Tabak, B.M. Multifractal Cross-Correlations of Dirty and Clean Cryptocurrencies with main financial indices. *Physica A* **2025**, *668*, 130541. <https://doi.org/https://doi.org/10.1016/j.physa.2025.130541>.
79. Li, J.C.; Xu, Y.Z.; Tao, C.; Zhong, G.Y. Multi-period impacts and network connectivity of cryptocurrencies to international stock markets. *Physica A* **2025**, *658*, 130299. <https://doi.org/https://doi.org/10.1016/j.physa.2024.130299>.
80. Nguyen, A.P.N.; Crane, M.; Conlon, T.; Bezbradica, M. Herding unmasked: Insights into cryptocurrencies, stocks and US ETFs. *PloS one* **2025**, *20*, e0316332. <https://doi.org/10.1371/journal.pone.0316332>.
81. Bouri, E.; Gupta, R.; Vo, X.V. Jumps in Geopolitical Risk and the Cryptocurrency Market: The Singularity of Bitcoin. *Defence and Peace Economics* **2022**, *33*, 150–161. <https://doi.org/10.1080/10242694.2020.1848285>.
82. Hong, M.Y.; Yoon, J.W. The impact of COVID-19 on cryptocurrency markets: A network analysis based on mutual information. *PLoS ONE* **2022**, *17*. <https://doi.org/10.1371/journal.pone.0259869>.
83. Khalfaoui, R.; Gozgor, G.; Goodell, J.W. Impact of Russia-Ukraine war attention on cryptocurrency: Evidence from quantile dependence analysis. *Finance Research Letters* **2023**, *52*, 103365. <https://doi.org/10.1016/j.frl.2022.103365>.
84. Fang, Y.; Tang, Q.; Wang, Y. Geopolitical Risk and Cryptocurrency Market Volatility. *Emerging Markets Finance and Trade* **2024**, *60*, 3254–3270. <https://doi.org/10.1080/1540496X.2024.2343948>.

85. Poongodi, M.; Nguyen, T.N.; Hamdi, M.; Cengiz, K. Global cryptocurrency trend prediction using social media. *Information Processing and Management* **2021**, *58*, 102708. <https://doi.org/10.1016/j.ipm.2021.102708>.
86. Aharon, D.Y.; Demir, E.; Lau, C.K.M.; Zaremba, A. Twitter-Based uncertainty and cryptocurrency returns. *Research in International Business and Finance* **2022**, *59*, 101546. <https://doi.org/10.1016/j.ribaf.2021.101546>.
87. Oświęcimka, P.; Drożdż, S.; Kwapień, J.; Górski, A.Z. Effect of Detrending on Multifractal Characteristics. *Acta Physica Polonica A* **2013**, *123*, 597–603. <https://doi.org/10.12693/APhysPolA.123.597>.
88. Johnson, C.R. Hadamard products of matrices. *Linear and Multilinear Algebra* **1974**, *1*, 295–307. <https://doi.org/10.1080/03081087408817030>.
89. FitzGerald, C.H.; Horn, R.A. On Fractional Hadamard Powers of Positive Definite Matrices. *Journal of Mathematical Analysis and Applications* **1977**, *61*, 633–342. [https://doi.org/10.1016/0022-247X\(77\)90167-6](https://doi.org/10.1016/0022-247X(77)90167-6).
90. Wishart, J. The Generalised Product Moment Distribution in Samples from a Normal Multivariate Population. *Biometrika* **1928**, *20A*, 32–52. <https://doi.org/10.1093/biomet/20A.1-2.32>.
91. Wątorek, M.; Kwapień, J.; Drożdż, S. Financial return distributions: Past, present, and covid-19. *Entropy* **2021**, *23*, 884. <https://doi.org/10.3390/e23070884>.
92. Gopikrishnan, P.; Meyer, M.; Amaral, L.N.; Stanley, H.E. Inverse cubic law for the distribution of stock price variations. *The European Physical Journal B* **1998**, *3*, 139–140. <https://doi.org/10.1007/s100510050292>.
93. James, N.; Menzies, M.; Chan, J. Changes to the extreme and erratic behaviour of cryptocurrencies during COVID-19. *Physica A* **2021**, *565*, 125581. <https://doi.org/10.1016/j.physa.2020.125581>.
94. Drożdż, S.; Kwapień, J.; Wątorek, M. What is mature and what is still emerging in the cryptocurrency market? *Entropy* **2023**, *25*. <https://doi.org/10.1080/713665670>.
95. Tsallis, C. Nonadditive entropy and nonextensive statistical mechanics -an overview after 20 years. *Brazilian Journal of Physics* **2009**, *39*, 337–356. <https://doi.org/10.1590/s0103-97332009000400002>.
96. Tsallis, C.; Levy, S.V.F.; Souza, A.M.C.; Maynard, R. Statistical-Mechanical Foundation of the Ubiquity of Lévy Distributions in Nature. *Physical Review Letters* **1995**, *75*, 3589–3593. <https://doi.org/10.1103/physrevlett.75.3589>.
97. Drożdż, S.; Kwapień, J.; Oświęcimka, P.; Rak, R. The foreign exchange market: Return distributions, multifractality, anomalous multifractality and the Epps effect. *New Journal of Physics* **2010**, *12*, 105003. <https://doi.org/10.1088/1367-2630/12/10/105003>.
98. Drożdż, S.; Wójcik, M. Nature of order from random two-body interactions. *Physica A* **2001**, *301*, 291–300. [https://doi.org/10.1016/S0378-4371\(01\)00403-4](https://doi.org/10.1016/S0378-4371(01)00403-4).
99. Drożdż, S.; Kwapień, J.; Speth, J.; Wójcik, M. Identifying complexity by means of matrices. *Physica A* **2002**, *314*, 355–361. [https://doi.org/10.1016/S0378-4371\(02\)01066-X](https://doi.org/10.1016/S0378-4371(02)01066-X).
100. Guhr, T.; Kälber, B. A new method to estimate the noise in financial correlation matrices. *Journal of Physics A* **2003**, *36*, 3009. <https://doi.org/10.1088/0305-4470/36/12/310>.
101. A dataset of 140 exchange rates from the Binance exchange. <https://doi.org/10.18150/WPGY4R>.
102. Epps, T.W. Comovements in Stock Prices in the Very Short Run. *Journal of the American Statistical Association* **1979**, *74*, 291–298. <https://doi.org/10.1080/01621459.1979.10482508>.
103. Kwapień, J.; Drożdż, S.; Speth, J. Time scales involved in emergent market coherence. *Physica A* **2004**, *337*, 231–242. <https://doi.org/10.1016/j.physa.2004.01.050>.
104. Wątorek, M.; Drożdż, S.; Oświęcimka, P.; Stanuszek, M. Multifractal cross-correlations between the world oil and other financial markets in 2012–2017. *Energy Economics* **2019**, *81*, 874–885. <https://doi.org/10.1016/j.eneco.2019.05.015>.
105. Haken, H. *Synergetics: Introduction and Advanced Topics – Nonequilibrium Phase Transitions and Self-Organization in Physics, Chemistry and Biology*; Springer, 2004. <https://doi.org/10.1007/978-3-662-10184-1>.